Role of *O*-(2-^{18}F-Fluoroethyl)-L-Tyrosine PET for Differentiation of Local Recurrent Brain Metastasis from Radiation Necrosis

Norbert Galldiks[1,2], Gabriele Stoffels[1,3], Christian P. Filss[1,3], Marc D. Piroth[3,4], Michael Sabel[5], Maximilian I. Ruge[6], Hans Herzog[1,3], Nadim J. Shah[1,3], Gereon R. Fink[1,2], Heinz H. Coenen[1,3], and Karl-Josef Langen[1,3]

[1]Institute of Neuroscience and Medicine (INM-3,-4,-5), Forschungszentrum Jülich, Jülich, Germany; [2]Department of Neurology, University of Cologne, Cologne, Germany; [3]JARA-Brain Section, Jülich Aachen Research Alliance (JARA), Jülich, Germany; [4]Department of Radiation Oncology, RWTH Aachen University Hospital, Aachen, Germany; [5]Department of Neurosurgery, University Hospital Düsseldorf, Düsseldorf, Germany; and [6]Department for Stereotaxy and Functional Neurosurgery, University of Cologne, Cologne, Germany

The aim of this study was to investigate the potential of *O*-(2-^{18}F-fluoroethyl)-L-tyrosine (^{18}F-FET) PET for differentiating local recurrent brain metastasis from radiation necrosis after radiation therapy because the use of contrast-enhanced MRI for this issue is often difficult. **Methods:** Thirty-one patients (mean age ± SD, 53 ± 11 y) with single or multiple contrast-enhancing brain lesions (n = 40) on MRI after radiation therapy of brain metastases were investigated with dynamic ^{18}F-FET PET. Maximum and mean tumor-to-brain ratios (TBR_{max} and TBR_{mean}, respectively; 20–40 min after injection) of ^{18}F-FET uptake were determined. Time–activity curves were generated, and the time to peak (TTP) was calculated. Furthermore, time–activity curves of each lesion were assigned to one of the following curve patterns: (I) constantly increasing ^{18}F-FET uptake, (II) ^{18}F-FET uptake peaking early (TTP ≤ 20 min) followed by a plateau, and (III) ^{18}F-FET uptake peaking early (TTP ≤ 20 min) followed by a constant descent. The diagnostic accuracy of the TBR_{max} and TBR_{mean} of ^{18}F-FET uptake and the curve patterns for the correct identification of recurrent brain metastasis were evaluated by receiver-operating-characteristic analyses or Fisher exact test for 2 × 2 contingency tables using subsequent histologic analysis (11 lesions in 11 patients) or clinical course and MRI findings (29 lesions in 20 patients) as reference. **Results:** Both TBR_{max} and TBR_{mean} were significantly higher in patients with recurrent metastasis (n = 19) than in patients with radiation necrosis (n = 21) (TBR_{max}, 3.2 ± 0.9 vs. 2.3 ± 0.5, $P < 0.001$; TBR_{mean}, 2.1 ± 0.4 vs. 1.8 ± 0.2, $P < 0.001$). The diagnostic accuracy of ^{18}F-FET PET for the correct identification of recurrent brain metastases reached 78% using TBR_{max} (area under the ROC curve [AUC], 0.822 ± 0.07; sensitivity, 79%; specificity, 76%; cutoff, 2.55; P = 0.001), 83% using TBR_{mean} (AUC, 0.851 ± 0.07; sensitivity, 74%; specificity, 90%; cutoff, 1.95; $P < 0.001$), and 92% for curve patterns II and III versus curve pattern I (sensitivity, 84%; specificity, 100%; $P < 0.0001$). The highest accuracy (93%) to diagnose local recurrent metastasis was obtained when both a TBR_{mean} greater than 1.9 and curve pattern II or III were present (AUC, 0.959 ± 0.03; sensitivity, 95%; specificity, 91%; $P < 0.001$). **Conclusion:** Our findings suggest that the combined evaluation of the TBR_{mean} of ^{18}F-FET uptake and the pattern of the time–activity curve can differentiate local brain metastasis recurrence from radionecrosis with high accuracy. ^{18}F-FET PET may thus contribute significantly to the management of patients with brain metastases.

Key Words: radiation necrosis; stereotactic radiosurgery; recurrent brain metastasis; amino acid PET; ^{18}F-fluoroethyl-L-tyrosine (^{18}F-FET)

J Nucl Med 2012; 53:1367–1374
DOI: 10.2967/jnumed.112.103325

The improvement in the treatment of solid tumors has led to an increasing number of patients who experience brain metastases during the course of the disease. Stereotactic radiosurgery (SRS) and whole-brain radiation therapy (WBRT) are commonly used to treat brain metastases, and a growing percentage of patients live long enough to experience a local relapse of these metastases. Thus, the number of patients experiencing local recurrence of previously irradiated brain metastases can be expected to increase. Contrast-enhanced MRI is the method of choice for the evaluation of metastatic brain tumors. However, in many patients, the differentiation of local recurrent brain metastasis from radiation necrosis after radiotherapy (e.g., SRS or WBRT) using contrast-enhanced MRI is difficult (*1*). This problem necessitates novel diagnostic methods for the follow-up and management of patients with recurrent brain metastases.

In addition to MRI, PET using ^{18}F-FDG (*2*) has been considered for the evaluation of metastatic brain tumors, but the high physiologic glucose consumption of the brain and the variable glucose uptake of metastatic brain lesions limit its use. For example, in a study of 48 patients with

Received Jan. 19, 2012; revision accepted Apr. 2, 2012.
For correspondence or reprints contact: Norbert Galldiks, Institute of Neuroscience and Medicine, Forschungszentrum Jülich, 52425 Jülich, Germany.
E-mail: N.Galldiks@fz-juelich.de
Published online Aug. 7, 2012.

lung cancer and brain metastasis, 33% of the brain lesions showed hypometabolism on ^{18}F-FDG PET, although all primary lung lesions were hypermetabolic (*3*). Another study demonstrated that after SRS using a γ-knife, ^{18}F-FDG PET is not sensitive enough to differentiate viable brain metastases from radiation necrosis (*4*). A recent study, however, indicated that dual-phase imaging may improve the diagnostic accuracy of ^{18}F-FDG PET for the differentiation of recurrent brain metastasis from radiation necrosis (*5*). A limitation of that approach is the long time interval between PET scans (2–5.7 h). Therefore, alternative imaging methods are still of great interest.

Amino acid tracers are particularly useful for PET in neurooncology because of a high amino acid uptake in tumor tissue together with low uptake in normal brain tissue, resulting in an enhanced tumor–to–normal tissue contrast. Previously, it has been shown that PET using L-[*methyl*-^{11}C]methionine (^{11}C-MET) may be effective in differentiating recurrent metastatic brain tumor from radiation-induced changes with a sensitivity of 78% and a specificity of 100%, respectively (*6*). In a subsequent study (*7*) with a larger number of patients (n = 51), these findings could be confirmed, at least in part, with similar sensitivity (79%) but with lower specificity (75%). The use of ^{11}C-MET, however, remains restricted to centers with an on-site cyclotron because of the short half-life of the ^{11}C isotope (20 min). In contrast, amino acids labeled with ^{18}F (half-life, 110 min) such as *O*-(2-^{18}F-fluoroethyl)-L-tyrosine (^{18}F-FET) allow a more widespread use and can be distributed via the satellite concept as has been shown with the widely used ^{18}F-FDG (*8–11*). Several studies have demonstrated the clinical utility of ^{18}F-FET PET, especially in the diagnostics and therapy assessment of cerebral gliomas (*12–14*). The tracer exhibits high in vivo stability, low uptake in inflammatory tissue, and suitable uptake kinetics for clinical imaging (*15–17*). Contrast-enhancing nontumoral tissue on MRI, for example, due to radionecrosis, is usually negative on ^{18}F-FET PET (*14*). Furthermore, ^{18}F-FET uptake kinetics have been shown to provide valuable information for the differentiation of high-grade from low-grade gliomas and treatment-related changes in the brain tissue (*8,16–19*). In contrast, the role of ^{18}F-FET PET in the diagnostics and therapy assessment of cerebral metastases is not yet established, and only a few studies have reported on increased ^{18}F-FET uptake in cerebral metastases (*20,21*).

Accordingly, here we evaluated the clinical usefulness of ^{18}F-FET PET for the differentiation of local recurrent brain metastasis from radiation necrosis.

MATERIALS AND METHODS

Patients

Thirty-one patients with metastatic brain tumors (mean age ± SD, 53 ± 11 y; age range, 17–70 y; 26 women and 5 men), each with at least 1 contrast-enhancing lesion (n = 40) on cerebral MRI, were included in the study (Table 1). The patients were consecutively sent from 2005 to 2011 to our institute because of suggestive MRI findings such as newly contrast-enhancing lesions or progression of contrast enhancement at the site of the initial metastasis, in order to differentiate local recurrent brain metastasis from radiation necrosis using ^{18}F-FET PET. All patients had been previously treated with SRS (range of radiation dose, 8–25 Gy) and partly with WBRT (range of radiation dose, 20–30 Gy). The median interval between radiotherapy and PET was 11.5 mo. All patients gave written informed consent to the PET investigation.

Histopathologic results for definite diagnosis were available for 11 patients (11 lesions). For the remaining patients, diagnosis of recurrent brain metastasis or radiation necrosis was based on the clinical course and results of MRI in the further follow-ups. Recurrent disease was anticipated if a new contrast-enhancing lesion appeared at exactly the same site as the treated metastasis after initial complete response, if the treated metastasis grew during follow-up according to the Macdonald criteria (*22*) (increase of >25% in the pretreated volume on contrast-enhanced T1-weighted MR images), or if new neurologic deficits or an exacerbation of existing neurologic symptoms occurred. Radiation necrosis or unspecific posttherapeutic changes in the tissue were assumed when the lesions showed spontaneous shrinkage or remained stable in size on contrast-enhanced MRI after a long-term follow-up (median time, 12 mo) and neurologic deficits remained unchanged or no new neurologic symptoms occurred.

PET with ^{18}F-FET and Data Analysis

The amino acid ^{18}F-FET was produced via nucleophilic ^{18}F-fluorination with a specific radioactivity of greater than 200 GBq/μmol as described previously (*11*). The radiochemical yield of tracer was about 60%–65% at a radiochemical purity greater than 98%. The tracer was administered as isotonic neutral solution. According to the German guidelines for brain tumor imaging using labeled amino acid analogs, all patients fasted for at least 12 h before PET (*23*). Dynamic PET studies were acquired up to 50 min after intravenous injection of approximately 200 MBq of ^{18}F-FET on an ECAT EXACT HR+ scanner (Siemens Medical Systems, Inc.) in 3-dimensional mode (32 rings; axial field of view, 15.5 cm). The emission recording consisted of 16 time frames (1–5, 1 min; 6–10, 3 min; and 11–16, 5 min) covering the period up to 50 min after injection. For attenuation correction, transmission was measured with three ^{68}Ge/^{68}Ga rotating line sources. After correction for random and scattered coincidences and dead time, image data were obtained by filtered backprojection in Fourier space using the ECAT 7.2 software. The reconstructed image resolution was approximately 5.5 mm.

^{18}F-FET uptake in the tissue was expressed as standardized uptake value (SUV) by dividing the radioactivity (kBq/mL) in the tissue by the radioactivity injected per gram of body weight.

^{18}F-FET PET and contrast-enhanced MRI were coregistered using MPI tool software (version 6.48; ATV). The fusion results were inspected and, if necessary, adapted using anatomic landmarks. The region-of-interest (ROI) analysis was based on the summed PET data from 20 to 40 min after injection (*23*). The transaxial slices showing the highest ^{18}F-FET accumulation in the tumors were chosen for ROI analyses. ^{18}F-FET uptake in the unaffected brain tissue was determined by a larger ROI placed on the contralateral hemisphere in an area of normal-appearing brain tissue including white and gray matter (mean area ± SD, 1,651 ± 496 mm^2) (*23*). ^{18}F-FET uptake in the tumor (tumor ROI) was determined by a 2-dimensional auto-contouring process using a

TABLE 1
Patient Characteristics

Patient no.	Sex	Age (y)	Tumor origin	Histologic diagnosis	Previous treatment of brain metastasis	No. of PET lesions	Localization	TBR_{max}	TBR_{mean}	Pattern of ^{18}F-FET kinetic	TTP (min)	Histologic diagnosis after PET	Time (mos)... Between RT and PET	Time (mos)... Of follow-up after PET	Final diagnosis
1	F	45	Breast	DC	WBRT, SRS, OP	1	Left frontal	2.7	1.9	II	20	Yes	10	ND	Met
2	M	58	Lung	NSCLC	OP, SRS	1	L temporal	3.0	1.9	I	25	Yes	19	ND	N
3	F	63	Lung	NSCLC, adenocarcinoma	OP, SRS	1	L frontal	2.5	1.9	I	35	Yes	19	ND	N
4	F	61	Lung	NSCLC	WBRT, SRS	1	L parietal	1.7	1.6	I	30	Yes	9	ND	N
5	F	45	Breast	DC	WBRT, SRS	1	L temporal	2.4	1.7	I	35	Yes	6	ND	N
6	F	69	Breast	DC	SRS	1	L parietal occipital	2.5	1.9	I	35	Yes	60	ND	N
7	F	50	Breast	DC	OP, WBRT, SRS	1	L temporal	3.5	2.1	I	35	Yes	6	ND	Met
8	F	51	Breast	DC	OP, WBRT, SRS	1	R parietal	3.5	2.1	II	20	Yes	10	ND	Met
9	F	17	Bone (pelvis)	Ewing sarcoma	SRS	1	BS	4.1	2.7	III	4	Yes	11	ND	Met
10	F	57	Lung	NSCLC, adenocarcinoma	OP, SRS	1	L parietal	1.5	1.2	I	40	Yes	13	ND	Met
11	F	48	Lung	NSCLC, adenocarcinoma	WBRT	1	L frontal	2.7	2.1	II	20	Yes	11	ND	Met
12	M	50	Skin	MM	SRS	1	L occipital	3.7	2.4	II	17	No	16	Rec	Met
13	F	47	Lung	NSCLC, adenocarcinoma	OP, WBRT, SRS	1	L occipital	3.2	2.1	I	25	No	12	38	N
14	F	69	Lung	NSCLC	SRS	1	R parietal	2.2	1.7	I	40	No	11	7	N
15	F	53	Colon	Adenocarcinoma	OP, WBRT, SRS	1	R parietal	2.2	1.7	I	45	No	10	6	N
16	F	54	Breast	DC	WBRT, SRS	2	L cerebellar (1)	3.5	2.0	II	20	No	11	Rec	Met
							L cerebellar (2)	3.6	2.2	II	20				
17	F	64	Lung	SCLC	WBRT, SRS	2	L frontal	2.5	1.9	III	14	No	7	Rec	Met
							BS	2.3	1.8	II	14				
18	F	58	Lung	NSCLC, adenocarcinoma	SRS	1	R parietal	2.2	1.8	I	35	No	18	S	N
19	F	43	Lung	NSCLC, adenocarcinoma	OP, SRS	1	L parietal	2.8	2.0	II	11	No	23	Rec	Met
20	F	44	Lung	NSCLC, adenocarcinoma	OP, SRS	1	L parietal	1.8	1.6	I	45	No	11	16	N
21	F	44	Lung	SCLC	WBRT, SRS	1	L parietal occipital	2.4	1.9	I	40	No	23	S	N
22	F	58	Lung	NSCLC	WBRT, SRS	2	R parietal occipital	2.8	2.0	I	35	No	16	Rec	Met
							L temporal	2.4	1.8	II	17				
23	M	49	Lung	NSCLC, adenocarcinoma	WBRT, SRS	4	R cerebellar	3.1	1.9	I	40	No	12	S	N
							L frontal	1.9	1.7	I	40				
							R parietal occipital	1.8	1.6	I	40				
							L parietal occipital	1.6	1.5	I	30				
24	F	58	Breast	DC	SRS	1	L parietal	1.8	1.6	I	45	No	32	12	N
25	F	56	Lung	NSCLC	SRS	1	R occipital	2.6	1.8	I	25	No	7	36	N
26	F	58	Lung	SCLC	WBRT, SRS	1	L temporal	2.1	1.9	I	45	No	5	5	N
27	M	33	Skin	MM	OP, WBRT, SRS	3	R parietal occipital	3.7	2.4	III	17	No	4	2*	Met
							BS	2.6	2.0	II	17				
							R parietal	2.6	2.2	II	17				
28	F	55	Breast	DC	SRS	1	L parietal	5.8	3.1	II	17	No	NA	1*	Met
29	F	70	Breast	DC	SRS	1	R occipital	3.6	2.5	II	20	No	15	Rec	Met
30	F	53	Lung	NSCLC, adenocarcinoma	SRS	1	L frontal	2.4	1.9	I	35	No	12	S	N
31	M	53	Kidney	RCC	OP, SRS	2	L occipital	3.0	2.0	I	30	No	15	S	N
							L frontal	2.3	1.7	I	30				

*Patient died during follow-up.

RT = radiation therapy; DC = ductal carcinoma; OP = resection; ND = not determined; Met = metastasis; NSCLC = non small-cell lung cancer; N = necrosis; BS = brain stem; MM = malignant melanoma; Rec = at time of ^{18}F-FET PET clinical signs or MRI findings consistent with recurrent metastatic tumor; S = at time of ^{18}F-FET PET patient stable without new symptoms or MRI findings without signs of tumor progression; SCLC = small cell lung cancer; NA = not available; RCC = renal cell carcinoma;

tumor-to-brain ratio (TBR) of 1.6 or more. This cutoff is based on a biopsy-controlled study of cerebral gliomas in which a lesion-to-brain ratio of 1.6 best separated tumoral from peritumoral tissue (*24*). Furthermore, we determined the longest diameter of contrast enhancement on MRI and of ^{18}F-FET uptake (longest diameter of the tumor ROI) and the area of the tumor ROI (mm^2) on ^{18}F-FET PET scans.

Mean and maximum TBR (TBR_{mean} and TBR_{max}, respectively) were calculated by dividing the mean and maximum SUV of the tumor ROI by the mean SUV of normal brain in the ^{18}F-FET PET scan. Time–activity curves were generated by application of the ROIs of the lesions (20–40 min) to the entire dynamic dataset. Time to peak (TTP; time in minutes from the beginning of the dynamic acquisition up to the maximum SUV of the lesion) was determined. Furthermore, the time–activity curves of each lesion were assigned to one of the following curve patterns: (I) constantly increasing ^{18}F-FET uptake without identifiable peak uptake, (II) ^{18}F-FET uptake peaking early (TTP $\leq$ 20 min) followed by a plateau, and (III) ^{18}F-FET uptake peaking early (TTP $\leq$ 20 min) followed by a constant descent.

Statistical Analyses

Descriptive statistics are provided as mean and SD or as median and range. To compare 2 groups, the Student *t* test was used. The Mann–Whitney rank-sum test was used when variables were not normally distributed. *P* values of less than 0.05 were considered significant. The diagnostic performance of TBR values to differentiate local recurrent brain metastasis from radiation necrosis was assessed by receiver-operating-characteristic (ROC) curve analyses using the results of histopathology or of the clinical course as reference. The diagnostic performance of curve patterns alone to differentiate local recurrent brain metastasis from radiation necrosis was evaluated by Fisher exact test for 2 × 2 contingency tables.

For the combined ROC analysis of TBR_{mean} and curve patterns, patient data were assigned to 1 of 3 categories: recurrent metastasis unlikely (TBR_{mean} < optimal cutoff in ROC analysis and curve pattern I), recurrent metastasis suspected (TBR_{mean} > optimal cutoff or curve pattern II or III), or recurrent metastasis highly probable (TBR_{mean} > optimal cutoff and curve pattern II or III).

For ROC analyses of TBR values, decision cutoff was considered optimal when the product of paired values for sensitivity and specificity reached its maximum. In addition, the area under the ROC curve (AUC), its SE, and level of significance were determined as a measure of diagnostic quality. Statistical analysis was performed using SigmaPlot software (version 11.0; Systat Software Inc.) and PASW statistics software (release 18.0.3; SPSS Inc.).

RESULTS

Surgical intervention was performed in 11 patients with single lesions, and histopathology showed viable tumor tissue in 6 patients and necrosis with no viable tumor cells in 5 patients. Sixteen lesions in 12 patients without histologic evaluation were classified as radiation necrosis because the patients exhibited stable neurologic symptoms and no significant enlargement of the lesion was observed on follow-up MR images after a median of 12 mo. Because of clinical deterioration of neurologic symptoms or progression in size on contrast-enhanced MRI during follow-up, 13 lesions in 8 patients were classified as recurrent brain metastases (Table 1).

Comparison of Uptake Indices for Recurrent Brain Metastasis and Radiation Necrosis

The TBR_{max} and TBR_{mean} were significantly higher in patients with recurrent metastases (n = 19) than in patients with radiation necrosis (n = 21) (TBR_{max}, 3.2 ± 0.9 vs. 2.3 ± 0.5, $P < 0.001$; TBR_{mean}, 2.1 ± 0.4 vs. 1.8 ± 0.2, $P < 0.001$). No significant size differences between radiation-induced lesions and recurrent metastases (median area of the tumor ROI, 230 vs. 404 mm^2; P = 0.16) could be observed. The smallest lesion size on ^{18}F-FET PET was 6 mm (range of longest diameter of tumor ROIs, 6–51 mm).

ROC Analysis of TBR Values

The diagnostic accuracy of ^{18}F-FET PET TBR values for the correct identification of recurrent brain metastases reached 78% using TBR_{max} (AUC, 0.822 ± 0.07; sensitivity, 79%; specificity, 76%; cutoff, 2.55; P = 0.001) and 83% using TBR_{mean} (AUC, 0.851 ± 0.07; sensitivity, 74%; specificity, 90%; cutoff, 1.95; $P < 0.001$) (Table 2).

Evaluation of Curve Patterns

In 31 patients, time–activity curves of 40 lesions were assessed. Two lesions were present in 4 patients (patients 16, 17, 22, and 31), 3 lesions in 1 patient (patient 27), and 4 lesions in 1 patient (patient 23) (Table 1). Time–activity curve pattern I (Fig. 1, patient 24) was found in 24 lesions (60%) of 21 patients, pattern II (Fig. 1, patient 12) in 10 lesions (25%) of 9 patients, and pattern III (Fig. 1, patient 9) in 6 lesions (15%) of 4 patients (Table 1). A preliminary analysis of our dataset revealed that kinetic pattern type I occurred mainly in lesions that had been caused by radiation necrosis whereas patterns II and III were typical of recur-

TABLE 2
Results of Diagnostic Performance

Identification of recurrent metastatic brain tumor	TBR_{max} > 2.55	TBR_{mean} > 1.95	^{18}F-FET kinetic patterns II and III	^{18}F-FET kinetic patterns II and III in combination with TBR_{mean} > 1.95
Sensitivity	79%	74%	84%	95%
Specificity	76%	90%	100%	91%
Accuracy	78%	83%	92%	93%
AUC ± SE	0.822 ± 0.07	0.851 ± 0.07	—	0.959 ± 0.03
P	0.001	<0.001	<0.0001	<0.001

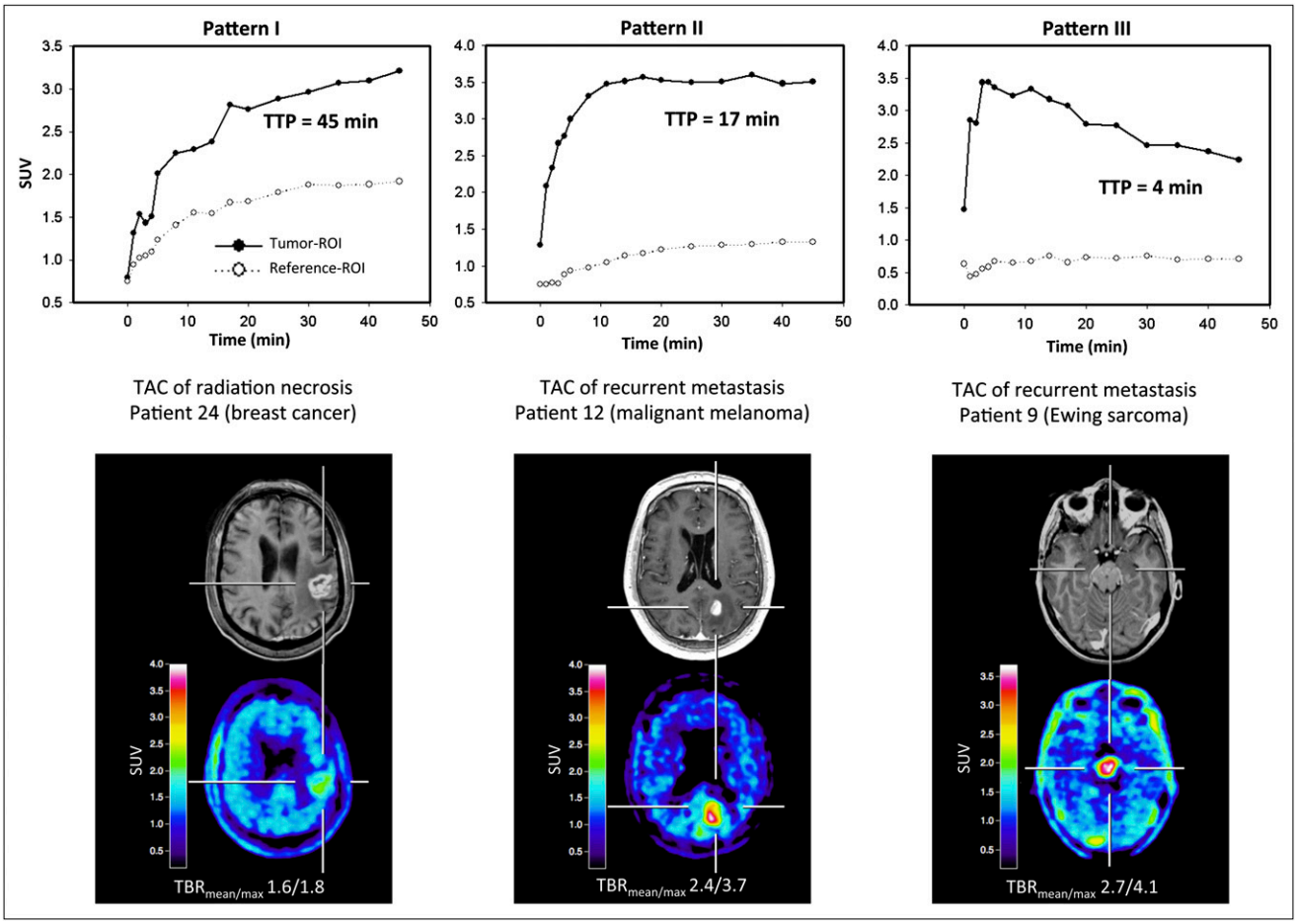

FIGURE 1. Examples of kinetics of radiation necrosis (pattern I) and recurrent brain metastasis (patterns II and III). All studies show pathologic contrast enhancement on T1-weighted MRI (minimal enhancement in patient 9) and corresponding increased ^{18}F-FET uptake (TBR_{mean} and TBR_{max} values are given below PET images). Dynamic evaluation of patient 24 (58-y-old woman 32 mo after SRS [brain metastasis of breast cancer, ductal carcinoma]) shows constantly increasing ^{18}F-FET uptake until end of acquisition. TTP is 45 min. Diagnosis of radiation necrosis was based on clinical course. Dynamic evaluation of patient 12 (50-y-old man 16 mo after SRS [brain metastasis of malignant melanoma]) shows early peak of ^{18}F-FET uptake (TTP = 17 min) followed by stable uptake until end of acquisition. Diagnosis of brain metastasis was based on clinical course. Dynamic evaluation of patient 9 (17-y-old girl, MRI findings and clinical course suggestive of first manifestation of metastatic brain tumor) shows early peak of ^{18}F-FET uptake after 4 min followed by constant decline of uptake until end of acquisition. Diagnosis of brain metastasis was confirmed histopathologically (Ewing sarcoma). TAC = time–activity curve.

rent brain metastasis. The diagnostic accuracy was 92% for curve patterns II and III versus curve pattern I (sensitivity, 84%; specificity, 100%; $P < 0.0001$).

Combined ROC Analysis of TBR_{mean} and Curve Pattern

The highest accuracy (93%) in diagnosing recurrent metastasis was obtained when both the TBR_{mean} was greater than 1.9 and the curve pattern was II or III (AUC, 0.959 ± 0.03; sensitivity, 95%; specificity, 91%; $P < 0.001$) (Table 2). Figure 2 shows the ROC curves for the TBR_{max}, TBR_{mean}, and combined use of TBR_{mean} and curve pattern for differentiation of local recurrent brain metastasis from radiation necrosis.

DISCUSSION

Cerebral metastases affect 20%–30% of all cancer patients and are the second most common form of cerebral neoplasm in adults. Today, the use of SRS is a widely accepted treatment option for cerebral metastases (*25*), either as a single modality or in combination with WBRT. Radiation-induced changes (i.e., radiation necrosis) on follow-up MRI studies including alterations in T2-weighted images and changing patterns of contrast enhancement have been reported in about 20% of all patients and can often not be distinguished from local tumor recurrence (*26–28*). The current gold standard for distinguishing tumor recurrence from radiation necrosis remains biopsy, which has an accuracy of more than 95% (*29,30*). Biopsy, however, is invasive and has potential complications such as infection, procedure-associated new neurologic problems, and hematoma, although the risk of permanent complications is relatively low (*29,30*). Therefore, a noninvasive imaging technique is desirable to derive valuable additional information.

As outlined here, the use of standard ^{18}F-FDG PET for the differentiation of tumor recurrence from radiation ne-

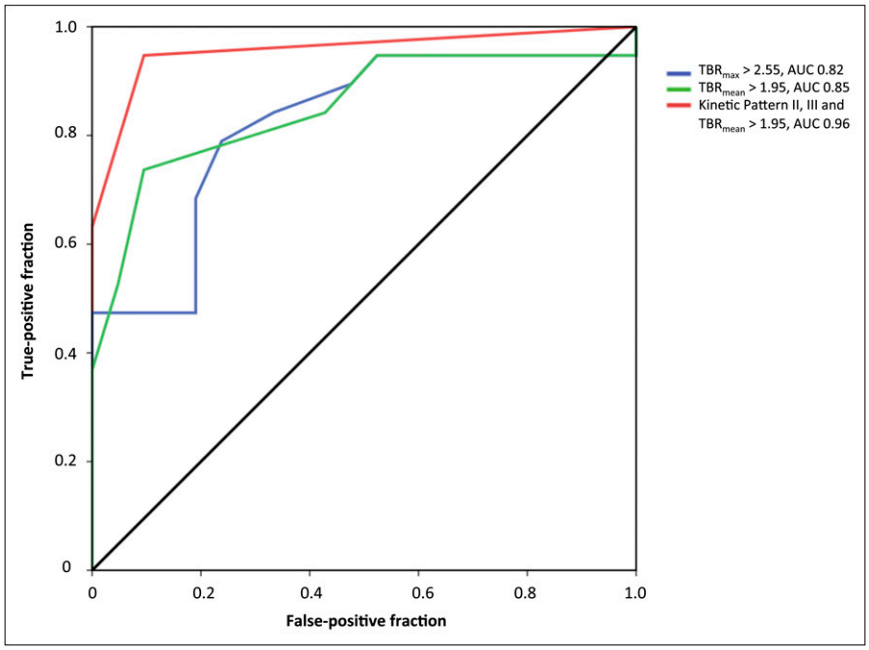

FIGURE 2. ROC curves for TBR_{max}, TBR_{mean}, and combined use of TBR_{mean} and curve pattern for metastatic brain tumors. AUC was 0.82 for TBR_{max} (blue line; optimal threshold > 2.55), 0.85 for TBR_{mean} (green line; optimal threshold > 1.95), and 0.96 for combination of kinetic patterns II and III and TBR_{mean} > 1.95 (red line).

crosis is unsatisfactory (*3,4*) but may be improved by dual-phase imaging (*5*). Differentiation using ^{11}C-MET PET could be achieved at a TBR_{mean} threshold of 1.41, with a sensitivity and specificity of 75% and 78%, respectively (*7*). Although this result is better than the performance of standard ^{18}F-FDG PET, it may still not be sufficient for clinical decision making. In the present study, we observed at a cutoff TBR_{mean} of 1.95 with ^{18}F-FET PET a similar sensitivity (74%) and improved specificity (90%). When our data are compared with the results using ^{11}C-MET PET (*7*), different cutoff values may be explained by methodologic differences in the generation of ROIs for the tumor and the background area. Another cause may be differences in the metabolic properties of the 2 different amino acids. Thus, ^{18}F-FET PET, compared with ^{11}C-MET PET, shows not only considerable logistic advantages but also improved accuracy in differentiating local recurrent brain metastasis from radionecrosis.

In addition to the diagnostic value of the TBR of ^{18}F-FET uptake, several studies have shown that the evaluation of ^{18}F-FET kinetics may add relevant diagnostic information, especially for noninvasive tumor grading and the differentiation of recurrent high-grade glioma from radiation necrosis (*8,16–19*). Time–activity curves of high-grade gliomas are characterized by an early peak of ^{18}F-FET uptake followed by a constant descent, whereas low-grade gliomas and benign brain lesions typically show a steadily increasing curve pattern. In contrast, ^{11}C-MET PET studies showed no different curve patterns in high- and low-grade gliomas (*31*).

To explore the putative impact of ^{18}F-FET kinetics, we analyzed time–activity curve patterns of ^{18}F-FET uptake in recurrent metastasis and radiation necrosis. A preliminary evaluation indicated that radiation necroses typically showed a steadily increasing curve pattern as previously reported for low-grade gliomas or benign posttherapeutic changes (curve pattern I), whereas curve patterns in recurrent metastases typically showed an early peak of ^{18}F-FET uptake followed by either a plateau (curve pattern II) or a constant descent (curve pattern III). Differentiation of local recurrent metastasis from radiation necrosis could be achieved with a sensitivity and specificity of 84% and 100%, respectively, when these different curve patterns were used as a diagnostic parameter. The highest accuracy in diagnosing recurrent metastases was obtained when both a pathologic TBR_{mean} and a type II or III curve pattern was present.

To the best of our knowledge, this is the first study exploring the usefulness of dynamic ^{18}F-FET PET for the differentiation of local recurrent brain metastasis from radiation necrosis. This approach may achieve an accuracy that is sufficient to influence clinical decision making and may therefore help to reduce the number of invasive diagnostic interventions and overtreatment in a considerable number of seriously ill patients with brain metastases. Limitations may be the relatively long scanning time (50 min), which may cause artifacts due to patient's head motion. This problem, however, did not occur in our study.

To date, experience with ^{18}F-FET PET in patients with brain metastases is limited, and ^{18}F-FET kinetics in the lesions have not yet been considered (*20,21*). Grosu et al. (*21*) reported for patients with confirmed recurrent brain metastases (clinically or through biopsy) after treatment with SRS (n = 9) a mean ^{18}F-FET uptake of 2.1 ± 0.6. In 4 patients with a final diagnosis of radiation injury, the mean ^{18}F-FET uptake was 1.5 ± 0.3. Pichler et al. (*20*) observed a mean ^{18}F-FET uptake of 2.7 ± 1.8 in 3 patients with histologically confirmed brain metastasis (lung cancer,

seminoma, and malignant melanoma). These results are in line with the results of the TBR values in our study and suggest that ^{18}F-FET PET may also be an option for the differentiation of recurrent brain metastases and nonneoplastic lesions.

Several factors may contribute to the different kinetic behaviors in recurrent brain metastasis and radiation necrosis. Weckesser et al. (*8*) suggested that the higher initial uptake in high-grade gliomas might be due to a higher regional blood volume as a consequence of increased angiogenesis and intratumoral microvessel density in patients with malignant progression (*32*). Accordingly, angiogenesis has long been established as a key element in the pathophysiology of development and growth of brain metastasis (*33*). Another explanation (*34*) may be an upregulation of facilitated amino acid transport, which is responsible for an increased ^{18}F-FET uptake in gliomas (*35*). An increased expression of sodium-independent L-type amino acid transporters has also been reported for metastatic tumor cells, for example, squamous cell carcinoma and adenocarcinoma (*36*). Most probably, the tracer kinetics in recurrent brain metastasis and radiation necrosis may be caused by both differences in vascularity and a differential expression of amino acid transporters that influence tracer influx and efflux. That both factors are likely to contribute to different kinetic patterns in brain metastasis is further supported by the finding that amino acid uptake has been shown to correlate with vascular density and microvessel density (*37,38*). In addition, SRS-induced effects (e.g., antiangiogenic effect) resulted in a change of the kinetic pattern (Fig. 3).

Although conventional MRI cannot reliably distinguish between recurrent brain metastasis and radiation necrosis, several advanced MRI techniques are presently evaluated that may eventually help to overcome this problem. For example, the value of multivoxel proton magnetic resonance spectroscopic imaging and dynamic susceptibility-weighted contrast-enhanced perfusion MRI has been successfully investigated (*39,40*). From both the patients' and the clinicians' perspective, the results are promising, but the clinical relevance of these methods is not yet established. These developments are, however, encouraging, and comparative studies are needed to investigate the relationship, diagnostic performance, and complementary character of amino acid PET and modern MRI techniques.

Because of the small sample size, the results of our study should be considered cautiously, and a larger prospective study is needed to confirm the clinical usefulness of ^{18}F-FET PET–derived imaging parameters for differentiating local recurrent brain metastasis from radiation necrosis after radiation therapy.

CONCLUSION

Our findings suggest that the TBR_{mean} and results of kinetic studies in ^{18}F-FET PET can differentiate local recurrent brain metastasis from radiation necrosis with a high sensitivity and specificity. ^{18}F-FET PET may thus contribute significantly to the management of patients with brain metastases.

DISCLOSURE STATEMENT

The costs of publication of this article were defrayed in part by the payment of page charges. Therefore, and solely to indicate this fact, this article is hereby marked "advertisement" in accordance with 18 USC section 1734.

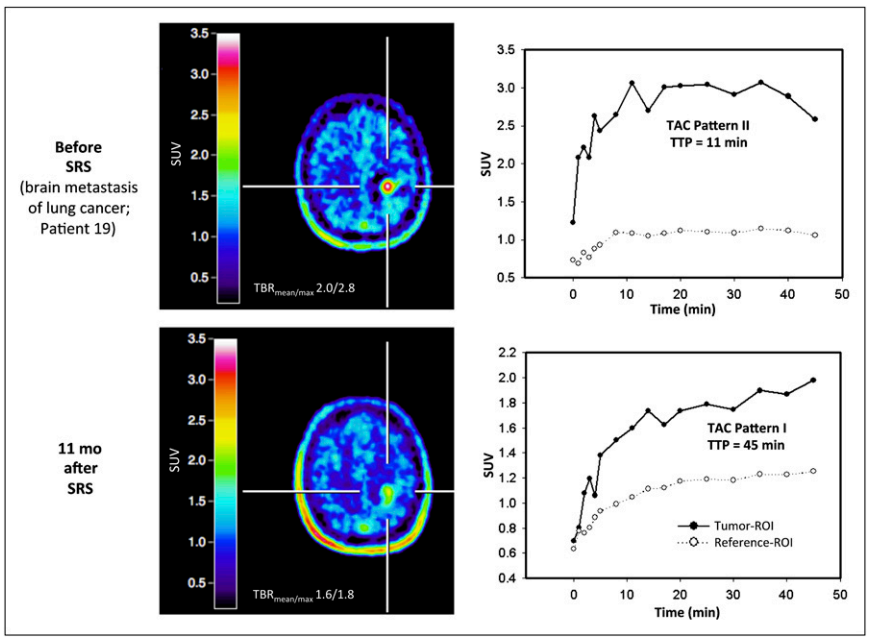

FIGURE 3. In patient 19, with lung cancer, γ-knife SRS of left parietal metastasis induced change in kinetic pattern of ^{18}F-FET uptake. Before SRS, values of TBR_{mean} and TBR_{max} were 2.0 and 2.8, respectively, and ^{18}F-FET uptake peaked early after 11 min and then stabilized (kinetic pattern II; top). Eleven months after SRS, values of TBR_{mean} and TBR_{max} declined (1.6 and 1.8, respectively), and ^{18}F-FET uptake pattern constantly increased (pattern I; bottom), indicating treatment response. TTP is 45 min. Sixteen months later, patient was still alive and without clinical signs of tumor recurrence. TAC = time–activity curve.

ACKNOWLEDGMENT

No potential conflict of interest relevant to this article was reported.

REFERENCES

1. Dooms GC, Hecht S, Brant-Zawadzki M, Berthiaume Y, Norman D, Newton TH. Brain radiation lesions: MR imaging. *Radiology.* 1986;158:149–155.
2. Di Chiro G, DeLaPaz RL, Brooks RA, et al. Glucose utilization of cerebral gliomas measured by [^{18}F]fluorodeoxyglucose and positron emission tomography. *Neurology.* 1982;32:1323–1329.
3. Lee HY, Chung JK, Jeong JM, et al. Comparison of FDG-PET findings of brain metastasis from non-small-cell lung cancer and small-cell lung cancer. *Ann Nucl Med.* 2008;22:281–286.
4. Belohlávek O, Simonova G, Kantorova I, Novotny J Jr, Liscak R. Brain metastases after stereotactic radiosurgery using the Leksell gamma knife: can FDG PET help to differentiate radionecrosis from tumour progression? *Eur J Nucl Med Mol Imaging.* 2003;30:96–100.
5. Horky LL, Hsiao EM, Weiss SE, Drappatz J, Gerbaudo VH. Dual phase FDG-PET imaging of brain metastases provides superior assessment of recurrence versus post-treatment necrosis. *J Neurooncol.* 2011;103:137–146.
6. Tsuyuguchi N, Sunada I, Iwai Y, et al. Methionine positron emission tomography of recurrent metastatic brain tumor and radiation necrosis after stereotactic radiosurgery: is a differential diagnosis possible? *J Neurosurg.* 2003;98:1056–1064.
7. Terakawa Y, Tsuyuguchi N, Iwai Y, et al. Diagnostic accuracy of ^{11}C-methionine PET for differentiation of recurrent brain tumors from radiation necrosis after radiotherapy. *J Nucl Med.* 2008;49:694–699.
8. Weckesser M, Langen KJ, Rickert CH, et al. O-(2-[^{18}F]fluorethyl)-L-tyrosine PET in the clinical evaluation of primary brain tumours. *Eur J Nucl Med Mol Imaging.* 2005;32:422–429.
9. Langen KJ, Hamacher K, Weckesser M, et al. O-(2-[^{18}F]fluoroethyl)-L-tyrosine: uptake mechanisms and clinical applications. *Nucl Med Biol.* 2006;33:287–294.
10. Wester HJ, Herz M, Weber W, et al. Synthesis and radiopharmacology of O-(2-[^{18}F]fluoroethyl)-L-tyrosine for tumor imaging. *J Nucl Med.* 1999;40:205–212.
11. Hamacher K, Coenen HH. Efficient routine production of the ^{18}F-labelled amino acid O-2-^{18}F fluoroethyl-L-tyrosine. *Appl Radiat Isot.* 2002;57:853–856.
12. Floeth FW, Pauleit D, Sabel M, et al. Prognostic value of O-(2-^{18}F-fluoroethyl)-L-tyrosine PET and MRI in low-grade glioma. *J Nucl Med.* 2007;48:519–527.
13. Piroth MD, Pinkawa M, Holy R, et al. Prognostic value of early [^{18}F]fluoroethyltyrosine positron emission tomography after radiochemotherapy in glioblastoma multiforme. *Int J Radiat Oncol Biol Phys.* 2011;80:176–184.
14. Pöpperl G, Götz C, Rachinger W, Gildehaus FJ, Tonn JC, Tatsch K. Value of O-(2-[^{18}F]fluoroethyl)-L-tyrosine PET for the diagnosis of recurrent glioma. *Eur J Nucl Med Mol Imaging.* 2004;31:1464–1470.
15. Salber D, Stoffels G, Pauleit D, et al. Differential uptake of O-(2-^{18}F-fluoroethyl)-L-tyrosine, L-^{3}H-methionine, and ^{3}H-deoxyglucose in brain abscesses. *J Nucl Med.* 2007;48:2056–2062.
16. Kunz M, Thon N, Eigenbrod S, et al. Hot spots in dynamic ^{18}FET-PET delineate malignant tumor parts within suspected WHO grade II gliomas. *Neuro-oncol.* 2011;13:307–316.
17. Pöpperl G, Kreth FW, Herms J, et al. Analysis of ^{18}F-FET PET for grading of recurrent gliomas: is evaluation of uptake kinetics superior to standard methods? *J Nucl Med.* 2006;47:393–403.
18. Calcagni ML, Galli G, Giordano A, et al. Dynamic O-(2-[^{18}F]fluoroethyl)-L-tyrosine (F-18 FET) PET for glioma grading: assessment of individual probability of malignancy. *Clin Nucl Med.* 2011;36:841–847.
19. Pöpperl G, Kreth FW, Mehrkens JH, et al. FET PET for the evaluation of untreated gliomas: correlation of FET uptake and uptake kinetics with tumour grading. *Eur J Nucl Med Mol Imaging.* 2007;34:1933–1942.
20. Pichler R, Dunzinger A, Wurm G, et al. Is there a place for FET PET in the initial evaluation of brain lesions with unknown significance? *Eur J Nucl Med Mol Imaging.* 2010;37:1521–1528.
21. Grosu AL, Astner ST, Riedel E, et al. An interindividual comparison of O-(2-[^{18}F]fluoroethyl)-L-tyrosine (FET)- and L-[methyl-^{11}C]methionine (MET)-PET in patients with brain gliomas and metastases. *Int J Radiat Oncol Biol Phys.* 2011;81:1049–1058.
22. Macdonald DR, Cascino TL, Schold SC Jr, Cairncross JG. Response criteria for phase II studies of supratentorial malignant glioma. *J Clin Oncol.* 1990;8:1277–1280.
23. Langen KJ, Bartenstein P, Boecker H, et al. German guidelines for brain tumour imaging by PET and SPECT using labelled amino acids. *Nuklearmedizin.* 2011;50:167–173.
24. Pauleit D, Floeth F, Hamacher K, et al. O-(2-[^{18}F]fluoroethyl)-L-tyrosine PET combined with MRI improves the diagnostic assessment of cerebral gliomas. *Brain.* 2005;128:678–687.
25. Suh JH. Stereotactic radiosurgery for the management of brain metastases. *N Engl J Med.* 2010;362:1119–1127.
26. Peterson AM, Meltzer CC, Evanson EJ, Flickinger JC, Kondziolka D. MR imaging response of brain metastases after gamma knife stereotactic radiosurgery. *Radiology.* 1999;211:807–814.
27. Ross DA, Sandler HM, Balter JM, Hayman JA, Archer PG, Auer DL. Imaging changes after stereotactic radiosurgery of primary and secondary malignant brain tumors. *J Neurooncol.* 2002;56:175–181.
28. Shaw E, Scott C, Souhami L, et al. Single dose radiosurgical treatment of recurrent previously irradiated primary brain tumors and brain metastases: final report of RTOG protocol 90-05. *Int J Radiat Oncol Biol Phys.* 2000;47:291–298.
29. Heper AO, Erden E, Savas A, et al. An analysis of stereotactic biopsy of brain tumors and nonneoplastic lesions: a prospective clinicopathologic study. *Surg Neurol.* 2005;64(suppl 2):S82–88.
30. Kreth FW, Muacevic A, Medele R, Bise K, Meyer T, Reulen HJ. The risk of haemorrhage after image guided stereotactic biopsy of intra-axial brain tumours: a prospective study. *Acta Neurochir (Wien).* 2001;143:539–545.
31. Moulin-Romsée G, D'Hondt E, de Groot T, et al. Non-invasive grading of brain tumours using dynamic amino acid PET imaging: does it work for ^{11}C-methionine? *Eur J Nucl Med Mol Imaging.* 2007;34:2082–2087.
32. Gupta K, Radotra BD, Banerjee AK, Nijhawan R. Quantitation of angiogenesis and its correlation with vascular endothelial growth factor expression in astrocytic tumors. *Anal Quant Cytol Histol.* 2004;26:223–229.
33. Fidler IJ, Ellis LM. The implications of angiogenesis for the biology and therapy of cancer metastasis. *Cell.* 1994;79:185–188.
34. Miyagawa T, Oku T, Uehara H, et al. "Facilitated" amino acid transport is upregulated in brain tumors. *J Cereb Blood Flow Metab.* 1998;18:500–509.
35. Heiss P, Mayer S, Herz M, Wester HJ, Schwaiger M, Senekowitsch-Schmidtke R. Investigation of transport mechanism and uptake kinetics of O-(2-[^{18}F]fluoroethyl)-L-tyrosine in vitro and in vivo. *J Nucl Med.* 1999;40:1367–1373.
36. Haase C, Bergmann R, Fuechtner F, Hoepping A, Pietzsch J. L-type amino acid transporters LAT1 and LAT4 in cancer: uptake of 3-O-methyl-6-^{18}F-fluoro-L-dopa in human adenocarcinoma and squamous cell carcinoma in vitro and in vivo. *J Nucl Med.* 2007;48:2063–2071.
37. Kracht LW, Friese M, Herholz K, et al. Methyl-[^{11}C]-l-methionine uptake as measured by positron emission tomography correlates to microvessel density in patients with glioma. *Eur J Nucl Med Mol Imaging.* 2003;30:868–873.
38. Stockhammer F, Plotkin M, Amthauer H, van Landeghem FK, Woiciechowsky C. Correlation of F-18-fluoro-ethyl-tyrosin uptake with vascular and cell density in non-contrast-enhancing gliomas. *J Neurooncol.* 2008;88:205–210.
39. Barajas RF, Chang JS, Sneed PK, Segal MR, McDermott MW, Cha S. Distinguishing recurrent intra-axial metastatic tumor from radiation necrosis following gamma knife radiosurgery using dynamic susceptibility-weighted contrast-enhanced perfusion MR imaging. *AJNR.* 2009;30: 367–372.
40. Chernov MF, Hayashi M, Izawa M, et al. Multivoxel proton MRS for differentiation of radiation-induced necrosis and tumor recurrence after gamma knife radiosurgery for brain metastases. *Brain Tumor Pathol.* 2006;23:19–27.

JNM The Journal of NUCLEAR MEDICINE

Role of *O*-(2-^{18}F-Fluoroethyl)-l-Tyrosine PET for Differentiation of Local Recurrent Brain Metastasis from Radiation Necrosis

Norbert Galldiks, Gabriele Stoffels, Christian P. Filss, Marc D. Piroth, Michael Sabel, Maximilian I. Ruge, Hans Herzog, Nadim J. Shah, Gereon R. Fink, Heinz H. Coenen and Karl-Josef Langen

J Nucl Med. 2012;53:1367-1374.
Published online: August 7, 2012.
Doi: 10.2967/jnumed.112.103325

The Journal of Nuclear Medicine is published monthly.
SNMMI | Society of Nuclear Medicine and Molecular Imaging
1850 Samuel Morse Drive, Reston, VA 20190.
(Print ISSN: 0161-5505, Online ISSN: 2159-662X)

SNMMI SOCIETY OF NUCLEAR MEDICINE AND MOLECULAR IMAGING